Proc. Natl. Acad. Sci. USA
Vol. 91, pp. 2694–2698, March 1994
Physiology

Molecular and physiological alterations in murine ventricular dysfunction

(digital angiography/phospholamban/sarcoplasmic reticulum/Ca^{2+}-ATPase/heart failure)

HOWARD A. ROCKMAN*†, SATOKO ONO*, ROBERT S. ROSS*‡, LARRY R. JONES§, MOHSIN KARIMI§, VALMIK BHARGAVA‡, JOHN ROSS, JR.*, AND KENNETH R. CHIEN*¶‖

*Department of Medicine, ¶Center for Molecular Genetics, ‡Veterans Affairs Hospital–San Diego and the ‖American Heart Association–Bugher Foundation Center for Molecular Biology, University of California, San Diego, School of Medicine, La Jolla, CA 92093; and the §Department of Medicine and the Krannert Institute of Cardiology, Indiana University School of Medicine, Indianapolis, IN 46202.

Communicated by Y. C. Fung, December 2, 1993

ABSTRACT **The present study reports the development and characterization of a murine model of right ventricular dysfunction following graded constriction in the pulmonary artery via microsurgical approaches. To analyze *in vivo* ventricular function, a technique of x-ray contrast microangiography was developed to allow the quantitative analysis of ventricular volumes and of ejection fraction in normal and pressure-overloaded right ventricle. Severe, chronic pulmonary arterial banding for 14 days resulted in right ventricular dilatation and dysfunction, associated with right atrial enlargement, and angiographic evidence of tricuspid regurgitation. These effects were dependent on the extent of hemodynamic overload, since more moderate pulmonary arterial constriction resulted in hypertrophy with maintenance of right ventricular function. With severe pulmonary artery constriction, the murine right ventricle displays a failing heart phenotype including chamber dilation with reduced function that resembles right ventricular dysfunction in man during chronic pulmonary arterial hypertension. Northern and immunoblot analyses demonstrate a marked down-regulation of phospholamban mRNA and its corresponding protein with both levels of constriction, while a less pronounced but significant depression of sarcoplasmic reticulum Ca^{2+}-ATPase protein was observed with severe overload, suggesting that this pattern is an early genetic marker of ventricular dysfunction. By coupling mouse genetics with this murine model and the ability to assess cardiac function *in vivo*, one should be able to test the role of the down-regulation of phospholamban and other defined alterations in the cardiac muscle gene program in the onset of the failing heart phenotype.**

Cardiac muscle failure is one of the most important problems in cardiovascular medicine. Although the physiology of the failing heart has been the subject of intense scientific inquiry, relatively little is known regarding the signaling pathways within cardiac muscle cells which mediate the progression from compensatory hypertrophy to cardiac muscle dysfunction. Although ventricular chamber dilation with reduced myocardial shortening and contractile velocity (1), as well as abnormal Ca^{2+} handling, appear to be hallmarks of the end-stage failing human heart (2), the molecular pathways which lead to these distinct phenotypes are unclear. One of the difficulties has been the paucity of animal model systems for analysis of the effects of the manipulation of a set of genes on cardiac function in the intact animal.

Utilizing recent advances in microsurgical approaches to create a graded constriction in the pulmonary artery (PA), we have developed and characterized a murine model of right ventricle (RV) hypertrophy and failure. In addition, a technique for digitized microangiography was developed to allow the quantitative analysis of *in vivo* cardiac function, ventricular volumes, and ejection fraction in normal and pressure-overloaded murine myocardium. Severe, chronic pulmonary arterial banding for 14 days resulted in a reproducible dysfunction of the RV chamber, associated with dilation of the ventricular chamber, enlargement of the right atrium (RA), and angiographic evidence of tricuspid regurgitation. These effects were dependent on the extent of hemodynamic overload, since more moderate pulmonary arterial constriction resulted in hypertrophy with maintenance of RV function. Northern and immunoblot analyses indicate that the marked down-regulation of phospholamban mRNA and its corresponding protein at both levels of constriction, with a small but significant depression in sarcoplasmic reticulum (SR) Ca^{2+}-ATPase protein only with severe overload, provides an early genetic marker of ventricular dysfunction.

METHODS

Microsurgical Techniques. Adult mice (C57BL/6, Simonsen Laboratories, Gilroy, CA) were anesthetized with a mixture of ketamine (100 mg/kg, i.p.), xylazine (5 mg/kg, i.p.), and morphine (2.5 mg/kg, i.p.). Under a dissecting microscope mice were intubated and connected to a rodent ventilator (3, 4) and the chest was entered through the third intercostal space. The pericardium was opened, the PA was isolated, and a suture ligature placed around the vessel. The suture was tied against either a 25-gauge needle (moderate stenosis) or 26-gauge needle (severe stenosis) which was then rapidly removed. After PA banding the chest was closed, the pneumothorax was evacuated, and the mouse was extubated and allowed to recover from anesthesia. Sham-operated animals underwent the same surgical procedure except for PA constriction.

After 14 days of PA banding, the mice were anesthetized as previously and experiments were terminated with an overdose of pentobarbital (150 mg/kg, i.p.). Hearts were excised and the atria, RV free wall, septum, and left ventricle (LV) were carefully dissected under the dissecting microscope and weighed separately. Both atrial and ventricular tissues were frozen separately in liquid nitrogen for mRNA and protein extraction. Dry chamber weights were determined from dissected atrial and ventricular tissue set aside to air dry.

The publication costs of this article were defrayed in part by page charge payment. This article must therefore be hereby marked "*advertisement*" in accordance with 18 U.S.C. §1734 solely to indicate this fact.

Abbreviations: ANF, atrial natriuretic factor (atriopeptin); EF, ejection fraction; LV, left ventricle; MLC-2, myosin light chain 2; PA, pulmonary artery; RA, right atrium; RV, right ventricle; SR, sarcoplasmic reticulum.

†To whom reprint requests should be addressed at: Department of Medicine, Basic Science Building, 0613B, La Jolla, CA 92093.

The overall mortality rates, including surgical and postoperative deaths following recovery from anesthesia, were 20% and 40% for the two groups.

Myocyte Size. Hearts studied for cell size (sham, $n = 5$; banded, $n = 12$) were fixed by perfusion with 4% paraformaldehyde after diastolic arrest (4). Sections (1 mm) from the midwall region of the RV were selected for cell area determination; if cell cross sections were close to circular, there was a visible nucleus and unbroken cellular membrane with absence of tissue edema. Cell areas were measured by manually tracing the cell outline on an imaging system and were made by an observer blinded to the origin of samples. Approximately 150 cells per heart were counted.

Digital Contrast Microangiography. Fourteen days after surgery, mice were anesthetized and placed on a rodent ventilator. If necessary the heart rate was slowed to 180–200 beats per minute by using the specific sinus-node inhibitor ULFS-49, known to only affect heart rate and to have no direct negative inotropic effect (5). Angiographic images were acquired on 3/4-inch videotape under constant fluoroscopy (General Electric Fluoricon 300, 4.5-inch field; 1 inch = 2.54 cm) following injection of 120 μl of nonionic contrast into the jugular vein over a period of 1–2 sec in 30° right anterior oblique and 60° left anterior oblique projections. X-ray images were digitized at 30 frames per second with a resolution matrix of 512 × 512 pixels with 256 shades of gray, using a time base corrector and a Gould De Anza video processing system interfaced to a VAX 11/750 computer system. First-pass RV and levophase LV video-density curves were generated by using field-by-field subtraction of RV and LV regions of interest from the corresponding background region of interest; images were interlaced to provide a temporal resolution equivalent to 60 frames per second. Ejection fraction (EF) values were calculated from the maximal (end-diastole) and minimal (end-systole) values of each beat, excluding the first beat since the RV chamber was not completely filled. At least two and, if available, three beats were averaged providing that the range of EF for each beat did not exceed 10%. By these criteria 50% of sham (10/20), 50% of PA-banded 25-gauge (9/18), and 86% of PA-banded 26-gauge (12/14) groups were suitable for angiographic analysis.

Biventricular and LV end-diastolic volumes were obtained from traced biplane images using the area–length method after grid correction for magnification. RV end-diastolic volume was calculated by subtracting the LV end-diastolic volume and calculated septal volume (weight/1.05) from the biventricular end-diastolic volume.

Northern Blot Analysis. Total RNA was isolated from three or four pooled chambers by a modification of the acid guanidinium thiocyanate technique (RNAzol; Cinna/Biotecx Laboratories, Houston, TX). RNA (10 μg) was size-fractionated by denaturing gel electrophoresis, transferred to nylon membranes by capillary action, and hybridized with appropriate cDNA probes (3, 4). Quantitative evaluation of autoradiograms was performed by laser densitometry of bands; band intensities were normalized to the hybridization signal obtained with the 28S rRNA (LKB UltroScan Laser Densitometer; Pharmacia). Exposure times were chosen to obtain densitometric scans within the linear response range of the radiographic film. cDNA probes were specific for mRNAs encoding rat atriopeptin (atrial natriuretic factor, ANF; full-length, 658 nt of coding region), rat myosin light chain 2 (MLC-2; full-length, 640 nt of coding region), rabbit cardiac SR Ca^{2+}-ATPase (657 nt of 5′ coding region), rabbit cardiac phospholamban (507 nt of 5′ coding region), or mouse 28S rRNA (full-length, 5000 nt of coding region).

Immunoblot Analysis. Thirty to 50 mg of mouse RV tissue was homogenized in 300 μl of 10 mM $NaHCO_3$ buffer at 4°C, 600 μl of 20% SDS was added, and the homogenate was centrifuged at room temperature at 12,000 × *g* for 10 min. Protein concentration in the supernatant of the SDS extract was determined by the method of Lowry *et al.* (6). Fifty to 100 μg of protein from each sample was electrophoresed in an SDS/8% polyacrylamide gel and transferred electrophoretically to 0.2-μm-pore-size nitrocellulose membranes (7, 8). Blots were incubated with a 1:500 dilution of monoclonal antibody 2A7-A1 (generated to the cardiac isoform of the canine SR Ca^{2+} pump), 1:500 dilution of phospholamban monoclonal antibody 2D12 (generated to phospholamban peptide 2–25) (7), or polyclonal rabbit antibodies to canine cardiac calsequestrin (8), then labeled for counting of radioactivity as described (8). Protein extracts from each sample were run in multiple gels to confirm reproducibility of results.

Statistical Analysis. Variables measured are expressed as mean ± SD. Statistical significance of differences in mean values of physiological parameters from sham-operated and PA-banded animals was assessed by Student's *t* test. One-way ANOVA with Scheffé's *F* test was used to examine the effect of PA banding on changes in the various mRNA and protein levels (sham vs. moderate PA banding vs. severe PA banding); $P < 0.05$ was considered significant.

RESULTS AND DISCUSSION

Development of a Murine Model of RV Dysfunction During Chronic PA Banding. Although chronic banding of the mouse transverse thoracic aorta can lead to concentric LV hypertrophy, these mice do not progress to cardiac muscle failure after long-term pressure overload (3 months), most likely because this results in only a moderate hemodynamic burden on the LV. Several other investigators have used a model of PA constriction in other species to study the effects of hemodynamic overload on RV function and have also shown markedly decreased contractile performance in isolated papillary muscles (9) and in the intact ventricle of failing hearts (10). Accordingly, we developed a model of murine RV overload through PA banding via modification of previously described microsurgical approaches for *in vivo* cardiovascular surgery in mice.

Moderate chronic pressure overload on the right heart for 14 days resulted in significant increase in wall thickness of the RA and RV chambers (data not shown). Evidence for the development of RV hypertrophy after 14 days of moderate PA stenosis was demonstrated by the increase in both wet and dry weight of the RV free wall (PA banding vs. sham, 33.05 ± 4.85 vs. 16.04 ± 4.97 mg of wet weight, $P < 0.0005$, and 8.05 ± 1.18 vs. 4.46 ± 1.44 mg of dry weight, $P < 0.0005$). Normalized for differences in body weight, a 93% increase in wet and a 68% increase in dry RV weight/body weight ratio were observed in the hypertrophied hearts compared with sham-operated hearts. Similarly there was an increase in the weight of the RA with pressure overload (PA banding vs. sham, 6.83 ± 3.27 vs. 2.01 ± 0.52 mg of wet weight, $P < 0.001$, and 1.46 ± 0.71 vs. 0.70 ± 0.26 mg of dry weight, $P < 0.01$), indicating RA hypertrophy. The development of RV and RA hypertrophy was not associated with changes in body weight after 14 days of moderate PA constriction (body weight pre- vs. post-PA banding, 21.2 ± 2.6 vs. 21.9 ± 3.1 g, *P* not significant). Cross-sectional areas of myocytes in the RV midwall were analyzed in 5 sham-operated mice (728 cells counted) and 12 PA-banded mice (2055 cells counted) subjected to moderate stenosis. Mean cross-sectional cell area increased from 255.08 ± 41.54 to 339.99 ± 72.83 μm^2 ($P < 0.01$) in the hypertrophied ventricles. Thus, similar to the effects of pulmonary hypertension in man and other experimental animals, PA banding can induce morphological and physiological parameters of myocardial hypertrophy that are selective for the RV chamber.

Quantitative Digital Microangiography to Assess RV Dysfunction. To determine whether chronic PA banding would lead to RV dysfunction *in vivo*, the method of digital microangiography was developed in the mouse. Representative angiographic images at end of diastole and end of systole in a sham-operated and a PA-banded animal are shown in Fig. 1. We used an area–length subtraction method to determine RV end-diastolic volumes. This method for determination of RV volumes by subtraction of LV and septal volume from the biventricular volume avoids assumptions of RV geometry, which varies with the hemodynamic load. However, the small size of the RV in systole precluded use of the area–length method to determine the EF. Since no other method of determining *in vivo* EF exists for the mouse, we have validated the densitometric method in the rat with direct balloon studies of the LV, using the area–length method for comparison and showing good agreement with the densitometric method (11).

Other investigators have estimated the cardiac output and stroke volume in conscious and anesthetized mice by using microspheres and indicator dilution techniques (12). The calculated LV stroke volume in sham-operated animals from our data (stroke volume, 43.03 ± 15.86 μl per beat) is in reasonable agreement with their data (37.0 ± 6.0 μl per beat) in anesthetized mice and further supports this method of assessing *in vivo* ventricular function. Similar results have also been obtained in an excised, working whole-heart preparation from mouse (13).

To study the alterations in RV function with pressure overload, we developed and applied the technique of *in vivo* contrast microangiography to a separate group of mice subjected to either moderate or severe PA stenosis. The physiologic consequences of severe chronic pressure overload on the RV were quite different from the response to a moderate load. Whereas a similar degree of hypertrophy indicated by RV weight was induced in both groups (Fig. 2*A*), severe overload resulted in significant RV dilation and depression of RV function as shown by the increase in RV end-diastolic volume and fall in RV EF (Fig. 2 *B* and *C*). Therefore a moderate pressure load stimulus induced a physiologic response characterized by compensatory concentric hypertrophy without significant increase in mean chamber size. In contrast, failure of adequate compensatory mechanisms prevailed in response to a more profound hemodynamic burden and resulted in RV chamber dilation and decompensated RV function with reduced EF in the severe PA stenosis group.

Since it was not technically possible to reliably measure PA pressure in these animals the exact loading conditions at the

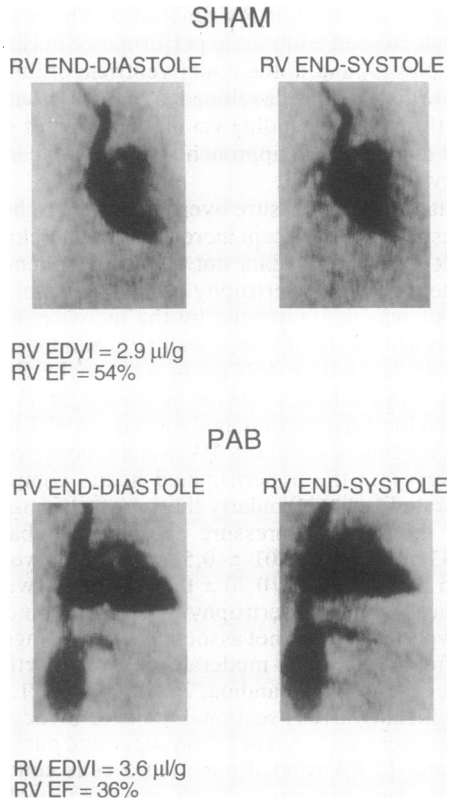

FIG. 1. Representative angiographic images demonstrating RV dilation and dysfunction following chronic PA banding (PAB). Increased RA and RV chamber size with retrograde filling of the dilated inferior vena cava with contrast is shown. Increased residual volume at end of systole indicates decreased EF and RV dysfunction. RV EDVI, RV end-diastolic volume/body weight.

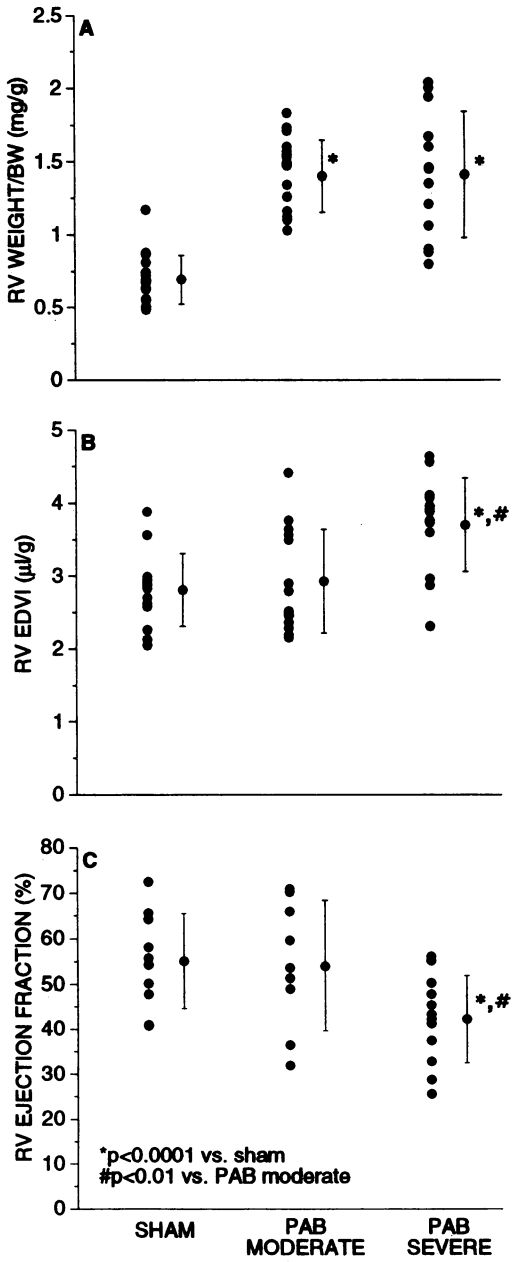

FIG. 2. Physiologic effects of moderate and severe RV overload. A significant increase in RV weight/body weight (BW) ratio occurred in response to both a moderate and a severe overload (*A*). Only hearts exposed to a severe overload dilated (increased angiographic RV end-diastolic volume/body weight ratio, EDVI) (*B*) and had a depressed EF (*C*). PAB, PA banding.

time of ventriculography could not be determined. It is therefore possible that the deterioration in ventricular function observed in the severe stenosis group was related, at least in part, to higher afterload rather than to a primary abnormality in myocardial contractility (afterload mismatch). This seems unlikely because (*i*) most of the mice with the tighter PA constriction developed significant tricuspid regurgitation and dilation of the inferior vena cava, which should tend to augment the EF due to the low-impedance backward leak, and (*ii*) studies in the cat subjected to RV overload have demonstrated contractile abnormalities at the isolated muscle level (14). Further studies are needed to confirm myocardial failure in this model of RV overload, using isolated muscle strips obtained from PA-banded mouse hearts.

Whether tricuspid regurgitation in the severe stenosis group actually contributed to the RV dilation is not known. It is possible that the hemodynamic effect on the RV was one of combined pressure and volume overload which resulted in ventricular dilation and pump failure. Finally, since wall stress is elevated in this model, it is possible that RV ischemia may have contributed to the ventricular dysfunction.

Genetic Markers of Ventricular Dysfunction. Studies of chronically dilated ventricles showing normal sarcomere lengths (15) and reduced contractile velocity (14) suggest an intrinsic abnormality of the contractile apparatus which, in part, may be related to alterations in myofilament Ca^{2+} availability and/or myofilament sensitivity to activator Ca^{2+} (16). Considerable attention has been devoted to the role of intracellular Ca^{2+} regulation and excitation–contraction coupling in heart failure. Studies in experimental and human end-stage heart failure have shown prolonged and abnormal intracellular Ca^{2+} transients recorded from aequorin-loaded muscle strips (2). These results, together with perturbations in excitation–contraction coupling as measured by a reduction in tension-independent heat (17), suggest that reduced Ca^{2+} release and removal are possible mechanisms to explain the defect in the failing myocardium. Recent studies in end-stage human heart failure have demonstrated decreased levels of SR Ca^{2+} ATPase (18), phospholamban (18, 19), and the Ca^{2+}-release channel (ryanodine receptor) (18) mRNAs, suggesting that transcriptional regulation of SR-related gene expression is altered in the failing human heart. However, in isolated SR vesicles from human failing myocardium no difference in Ca^{2+} uptake rates and phospholamban-mediated stimulation of Ca^{2+} uptake was observed compared with control hearts (20).

Accordingly, we examined alterations in genetic markers that are hallmarks of cardiac hypertrophy and failure in the clinical setting (21). As assessed by Northern blotting, a significant induction of ANF mRNA in the right ventricle occurred after PA banding. This was seen in ventricles subjected to either moderate or severe PA stenosis (Fig. 3). Phospholamban mRNA and protein were significantly decreased in both groups and appeared to follow a pattern of graded down-regulation, with the lowest levels of phospholamban protein seen with the greatest hemodynamic overload (Figs. 3 and 4). Although there was a downward trend, no statistically significant change in the level of SR Ca^{2+}-ATPase mRNA was detected in the RV after PA banding with either level of hemodynamic overload (Fig. 3). However, quantitative immunoblotting (Fig. 4) demonstrated a small but significant decrease in SR Ca^{2+}-ATPase protein compared with sham animals only with severe PA banding. Endogenous MLC-2 gene expression was shown to be similar in all three groups (Fig. 3).

Phospholamban is a pentameric phosphoprotein composed of five 52-aa monomeric subunits that acts as a regulator of SR Ca^{2+}-ATPase activity (22). Phosphorylation of phospholamban by cAMP-dependent protein kinase with β-adrenergic stimulation results in enhanced Ca^{2+} uptake through disinhibition of the Ca^{2+} pump (23, 24). Although it is not known whether alterations in transcription cause myocardial failure, several investigators have demonstrated a down-regulation of phospholamban and SR Ca^{2+}-ATPase gene expression in biopsy specimens from end-stage failing human hearts (18, 19), whereas a decrease in only SR Ca^{2+}-ATPase

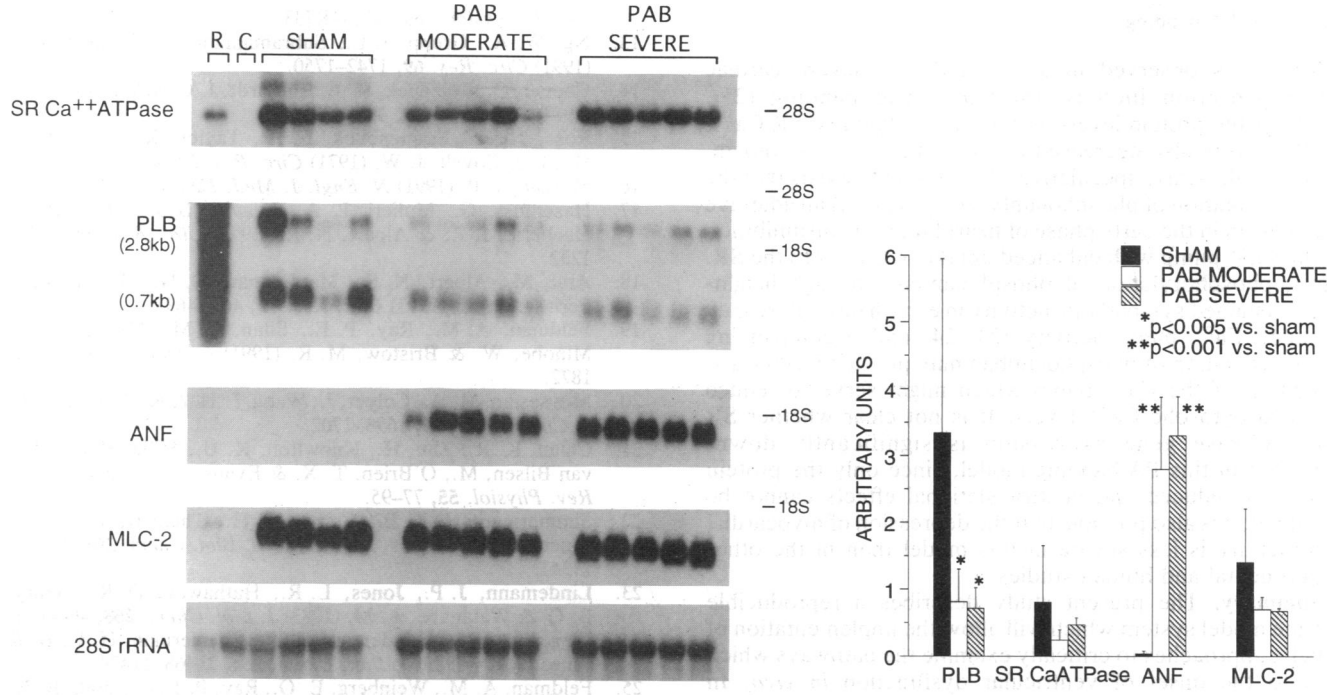

FIG. 3. (*Left*) Northern blot analysis showing the changes in mRNA levels in the RV during compensated hypertrophy and decompensated heart failure. PAB, PA banding; PLB, phospholamban. Lanes: R, rabbit LV; C, COS monkey cells (which do not contain SR Ca^{2+}-ATPase and thus serve as a negative control). (*Right*) Densitometric quantification of autoradiograms. No. of lanes scanned: sham, $n = 4$; PAB moderate, $n = 5$; PAB severe, $n = 5$. For PLB, upper and lower band signal intensity was used in the quantification.

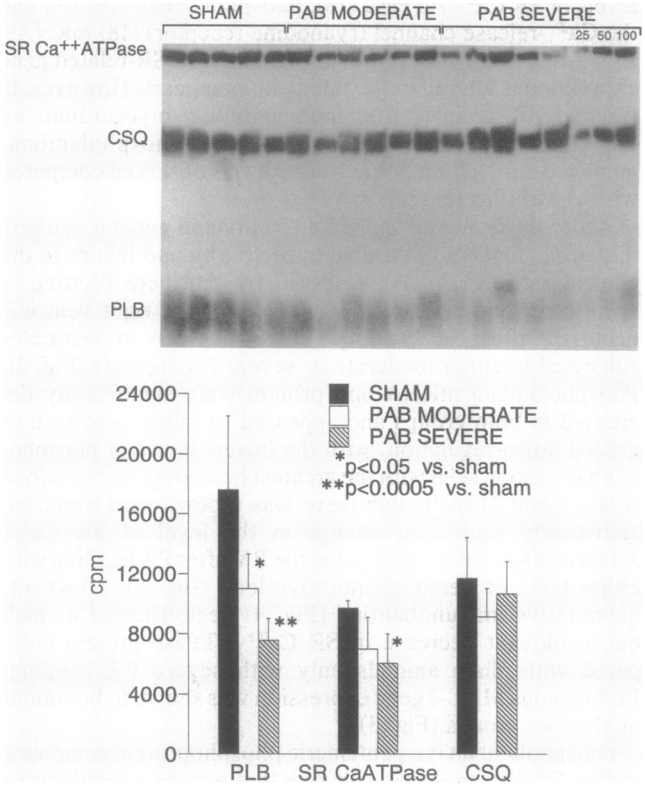

FIG. 4. (*Upper*) Immunoblot showing marked down-regulation of phospholamban and a small but significant decrease in SR Ca^{2+}-ATPase protein levels in failing RVs. Each lane represents a separate experiment except for the sham lanes, where two hearts were pooled. One hundred micrograms of total protein was loaded in each lane. Only the pentameric form of phospholamban, including both phosphorylated and dephosphorylated forms, is shown, since the signal for the monomer was below detection. For one sample, 25, 50, and 100 μg of protein was loaded to confirm a linear relationship with loading. (*Lower*) Quantitative immunoblotting was performed by scintillation counting of excised ^{125}I-labeled bands. CSQ, calsequestrin; PAB, PA banding.

mRNA was observed in a rat model of severe cardiac decompensation induced through aortic banding (25). Whether the protein levels of phospholamban and SR Ca^{2+}-ATPase were also decreased in those studies is not known.

Although clearly speculative, the possibility exists that the down-regulation of phospholamban may serve as an adaptive mechanism in the early phase of heart failure by disinhibition of the Ca^{2+} pump with enhanced uptake of Ca^{2+} into the SR. Thus, phosphorylation of phospholamban through heightened sustained sympathetic activity in early heart failure may enhance Ca^{2+} pump activity (23, 24) and accompanying down-regulation of phospholamban may provide further disinhibition of the Ca^{2+} pump which might serve to reduce elevated cytosolic Ca^{2+} levels. It is not clear whether SR Ca^{2+}-ATPase gene expression is significantly down-regulated in this PA-banding model, since only the protein level was reduced and posttranslational effects cannot be excluded; it is also possible that the depression of myocardial contractility is less severe in this model than in the other experimental and human studies.

Summary. The present study describes a reproducible murine model system which will allow the implementation of genetic approaches to critically examine the pathways which lead to the onset of ventricular dysfunction *in vivo*. In addition, a method employing quantitative digital microangiography has been developed to assess *in vivo* murine cardiac function and volumes; use of this method has documented the onset of RV dysfunction in these mice. This study demonstrates the feasibility of utilizing mouse genetics to identify the mechanisms which lead to the complex physiological transition between compensatory hypertrophy to overt cardiac muscle dysfunction and failure. In addition, the availability of miniaturized technology for catheterization and angiography in the mouse should be of widespread value in coupling *in vivo* cardiovascular physiology with mouse genetics (26).

We gratefully acknowledge Dr. David MacLennan for sharing cDNAs (SR Ca^{2+}-ATPase and phospholamban), Dr. Lan Mao for expert microsurgical assistance, and Carol Kent for expert technical assistance. This work was supported by National Institutes of Health Grant HL46345 (to K.R.C.), and a Grant-in-Aid from the American Heart Association, California Affiliate, no. 92-300 (to H.A.R.).

1. Katz, A. M. (1990) *N. Engl. J. Med.* **322,** 100–110.
2. Gwathmey, J. K., Copelas, L., MacKinnon, R., Schoen, F. J., Feldman, M. D., Grossman, W. & Morgan, J. P. (1987) *Circ. Res.* **61,** 70–76.
3. Rockman, H. A., Ross, R. S., Harris, A. N., Knowlton, K. U., Steinhelper, M. E., Field, L. J., Ross, J., Jr., & Chien, K. R. (1991) *Proc. Natl. Acad. Sci. USA* **88,** 8277–8281.
4. Rockman, H. A., Knowlton, K. U., Ross, J., Jr., & Chien, K. R. (1993) *Circulation* **87,** Suppl. VII, VII-14–VII-21.
5. Miura, T., Miyazaki, S., Guth, B., Kamayashi, M. & Ross, J., Jr. (1992) *Circulation* **86,** 563–571.
6. Lowry, O. H., Rosebrough, N. J., Farr, A. L. & Randall, R. J. (1951) *J. Biol. Chem.* **193,** 265–275.
7. Jones, L. R. & Field, L. J. (1993) *J. Biol. Chem.* **268,** 1–3.
8. Mahony, L. & Jones, L. R. (1986) *J. Biol. Chem.* **261,** 15257–15265.
9. Alpert, N. R. & Mulieri, L. A. (1982) *Circ. Res.* **50,** 491–500.
10. Spann, J. F., Jr., Covell, J. W., Eckberg, D. L., Sonnenblick, E. H., Ross, J., Jr., & Braunwald, E. (1972) *Am. J. Physiol.* **223,** 1150–1157.
11. Bhargava, V., Hagan, G., Miyamoto, M. I., Ono, S., Ono, S., Rockman, H. A. & Ross, J., Jr. (1992) *IEEE Computers in Cardiology* (IEEE Computer Soc., Los Alamitos, CA), pp. 191–194.
12. Barbee, R. W., Perry, B. D., Re, R. N. & Murgo, J. P. (1992) *Am. J. Physiol.* **263,** R728–R733.
13. Ng, W. A., Grupp, I. L., Subramaniam, A. & Robbins, J. (1991) *Circ. Res.* **69,** 1742–1750.
14. Cooper, G., Tomanek, R. J., Ehrhardt, J. C. & Marcus, M. L. (1981) *Circ. Res.* **48,** 488–497.
15. Ross, J., Jr., Sonnenblick, E. H., Taylor, R. R., Spotnitz, H. M. & Covell, J. W. (1971) *Circ. Res.* **28,** 49–61.
16. Morgan, J. P. (1991) *N. Engl. J. Med.* **325,** 625–632.
17. Hasenfuss, G., Mulieri, L. A., Leavitt, B. J., Allen, P. D., Haeberle, J. R. & Alpert, N. R. (1992) *Circ. Res.* **70,** 1225–1232.
18. Arai, M., Alpert, N. R., MacLennan, D. H., Barton, P. & Periasamy, M. (1993) *Circ. Res.* **72,** 463–469.
19. Feldman, A. M., Ray, P. E., Silan, C. M., Mercer, J. A., Minobe, W. & Bristow, M. R. (1991) *Circulation* **83,** 1866–1872.
20. Movsesian, M. A., Colyer, J., Wang, J. H. & Krall, J. J. (1990) *J. Clin. Invest.* **85,** 1698–1702.
21. Chien, K. R., Zhu, H., Knowlton, K. U., Miller-Hance, W., van Bilsen, M., O'Brien, T. X. & Evans, S. M. (1993) *Annu. Rev. Physiol.* **55,** 77–95.
22. Simmerman, H. K. B., Collins, J. H., Theibert, J. L., Wegener, A. D. & Jones, J. R. (1986) *J. Biol. Chem.* **261,** 13333–13341.
23. Lindemann, J. P., Jones, L. R., Hathaway, D. R., Henry, B. G. & Watanabe, A. M. (1983) *J. Biol. Chem.* **258,** 464–471.
24. Wegener, A. D., Lindemann, J. P., Simmerman, H. K. B. & Jones, J. R. (1989) *J. Biol. Chem.* **264,** 11468–11474.
25. Feldman, A. M., Weinberg, E. O., Ray, P. E. & Lorell, B. H. (1993) *Circ. Res.* **73,** 184–192.
26. Chien, K. R. (1993) *Science* **260,** 916–917.